Journal of Zhejiang University SCIENCE A
ISSN 1009-3095 (Print); ISSN 1862-1775 (Online)
www.zju.edu.cn/jzus; www.springerlink.com
E-mail: jzus@zju.edu.cn

Refined empirical line method to calibrate IKONOS imagery*

XU Jun-feng, HUANG Jing-feng†‡
(*Institute of Agricultural Remote Sensing and Information Technology, Zhejiang University, Hangzhou 310029, China*)
†E-mail: hjf@zju.edu.cn

Received Aug. 26, 2005; revision accepted Oct. 25, 2005

Abstract: To extract quantitative biophysical parameters such as leaf biomass and leaf chlorophyll concentration from the remotely sensed imagery, the effect of atmospheric attenuation must be removed. The refined empirical line (REL) method was used to calibrate the IKONOS multispectral imagery. The IKONOS digital numbers (DN) were converted to the at-satellite reflectance, then the linear relation between at-satellite reflectance and surface spectral reflectance (ρ_λ) was derived from six bright targets of known reflectance in the image, and modelled estimates of the image reflectance at ρ_λ=0. Validation targets were used to test the feasibility of REL method. The mean relative errors between ρ_λ retrieved from IKONOS image using REL method and ground-measured ρ_λ were 11%, 13%, 3% and 5% in the IKONOS blue, green, red and near-infrared (NIR) respectively. When dark targets are unavailable or measurement of dark target is inconvenient, the REL method was most crucial for retrieving surface spectral reflectance. The REL offers a simple approach for quantitative retrieval of biophysical parameters from IKONOS imagery.

Key words: Calibration, Refined empirical line (REL) method, IKONOS
doi:10.1631/jzus.2006.A0641 **Document code:** A **CLC number:** TP751

INTRODUCTION

To extract quantitative biophysical parameter such as leaf biomass and leaf chlorophyll concentration from the remotely sensed imagery accurately, the effects of atmospheric scattering and absorption must be removed. Atmospheric effects add to or diminish true ground reflectance, if the atmospheric spectral features are not properly removed. A significant analytical bias could be introduced for data interpretation (Ben-Dor and Levin, 2000).

Many approaches have been developed for atmospheric correction and calibration of surface reflectance of remotely sensed imagery (Roger and Gregg, 2002). These approaches may be grouped into four broad categories: (1) scene-derived corrections such as Internal Average Relative Reflectance (Kruse, 1988), (2) radiative transfer models (RTM) such as LOWTRAN (Kneizys *et al*., 1988), MODTRAN (Berk *et al*., 1998), 5S (Tanre, 1990), FLAASH (Matthew *et al*., 2002) and ATCOR (Richter and Schläpfer, 2002), (3) ground-calibration methods such as empirical line method (Farrand *et al*., 1994; Ferrier 1995), and (4) hybrid radiative-transfer-ground calibration procedures (Roger and Gregg, 2002).

The empirical line (EL) method assumes that the effects of the atmosphere are uniform across the image, and within the image are one or more targets with different reflectance characteristics covering a wide range of reflectance values for the wavebands recorded by the sensor (Smith and Milton, 1999). An empirical relationship between at-satellite reflectance and ground-measured (or estimated) reflectance ρ_λ can be derived (Fig.1a) when dark (lower reflectance) and bright (higher reflectance) targets are available and well characterized.

A refinement of the EL approach termed refined empirical line (REL) approach has been proposed, which resolves the difficulty dark and bright targets

‡ Corresponding author
* Project supported by the Hi-Tech Research and Development Program (863) of China (Nos. 2002AA130010-2-7 and 2003AA131020-04-06) and the National Natural Science Foundation of China (No. 40171065)

not being available (Moran *et al*., 2001). The REL approach derives the relation between at-satellite reflectance and ρ_λ based on two points: a single high-reflectance target within the scene and an estimate of the image reflectance associated with a surface of ρ_λ=0 (Fig.1b). The estimate of at-satellite reflectance for ρ_λ=0 is obtained through the use of an RTM with reasonable water and aerosol models, or measurements of atmospheric conditions on a typical cloud free day.

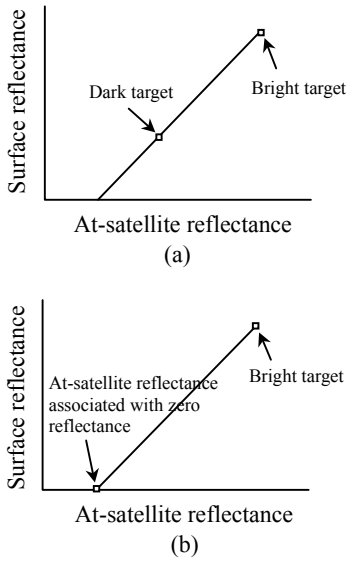

Fig.1 The prediction equations (a) from two calibration targets for the EL method and (b) from one target and a modelled at-satellite reflectance for ρ_λ=0 by RTM

In this study, the surface reflectance of 6 calibration and 5 validation targets were measured on the ground with a field spectrometer, and the corresponding reflectances are extracted from the image of these targets; the estimates of the IKONOS at-satellite reflectance for a surface ρ_λ=0 were computed for all the IKONOS bands in visible and near-infrared (NIR) bands (Table 1) by a RTM model. Image reflectance in each band and modelled reflectance are compared with the ground-measured reflectance to yield an empirical linear equation for predicting true reflectance.

Table 1 The four IKONOS multispectral bands

Spectral band name	Spectral band range (nm)
Blue	444.7~516.0
Green	506.4~595.0
Red	631.9~697.7
NIR	757.3~852.7

MATERIALS AND METHODS

An IKONOS multispectral image was acquired over Mountain Putuo on 31 March, 2002, at 02:32 GMT. Mountain Putuo, is actually a small island of the Zhoushan Archipelago in China. It contains a range of surface cover types including bright targets such as concrete road, sand and dam; and dark targets such as black rooftop and deep seawater. The study area is about 12 km^2 and spatial variation of atmosphere was small. Thus, the EL method can be applied to the area. The four IKONOS bands were converted to at-satellite reflectance ρ:

$$\rho=\frac{\pi\times(DN_\lambda/(CalCoef_\lambda/10))/Bandwidth_\lambda\times d^2}{ESUN_\lambda\times\cos\theta_s}, \quad (1)$$

where ρ is at-sensor reflectance, DN_λ is The IKONOS digital numbers, $CalCoef_\lambda$ is band dependent calibration coefficient, $ESUN_\lambda$ is band dependent mean solar exoatmospheric irradiance, d is earth-sun distance, in astronomical units, and θ_s is solar zenith angle (Fleming, 2003).

Field measurements

Surface reflectance measurements were made between 21 and 23 October, 2004. Measurements were taken between 10:00 and 14:00 hour local time under condition of clear skies. Because there were two years delay between the satellite imagery and ground measurements, the physical and chemical characteristics of some surface objects such as forest, grass and soil have changed. Spectrally stable objects were selected as REL targets. In this paper, 6 calibration (Table 2) and 4 validation targets (Table 3) were measured and characterized, including concrete floor, white sand, granite, plastic floor and black tile. The physical and chemical characteristics of these targets are quite stable over time and difficult to be weathered. Thus the targets are spectrally stable over time.

The calibration or validation targets should be large and homogeneous, so that, many spectra can be averaged to minimize noise in the flight data calibration. The 4-m spatial resolution of IKONOS facilitated finding of two or more homogenous contrasting reflectance targets large enough to be resolved (Karpouzli and Malthus, 2003; Perry *et al*., 2000).

Table 2 Description of calibration targets and mean coefficients of variation (CV) between spectra averaged

Calibration targets	Description	*CV* (%)
C1	Concrete floor of station	10.41
C2	Concrete floor of basketball ground	9.91
C3	White coastline sand on beach	4.68
C4	White coastline sand on beach	12.34
C5	Granite beside beach	16.91
C6	Green colored plastic floor of tennis court	8.53

Table 3 Description of validation targets and mean coefficients of variation (CV) between spectra averaged

Validation targets	Description	*CV* (%)
V1	White coastline sand on beach	5.34
V2	Dam face	9.62
V3	Concrete road	2.55
V4	Black tile on rooftop	6.25

Measurement of reflectance was taken on the ground for the calibration and validation targets using an Analytical Spectral Device (ASD) FieldSpec spectrometer, (333~1056 nm, spectral resolution: 3 nm). A sensor head was placed about 1 m above the targets. Twenty to thirty sampling spectra were taken for each target; each sampling spectrum consisted of 10 readings. Dark signal was subtracted and spectral data were compared to that of a standard white reference as spectral measurement. Spectral data were measured and account for their spatial variation; IKONOS spectral bands were simulated with the ASD FiedSpec data by integrating the 0.003 μm ASD data using the normalized spectral response curves for each IKONOS band.

A Trimble GeoXT^{TM} GPS unit with sub-meter accuracy, operated in real-time differential mode was used to collect Ground Control Points (GCPs). Subsequently the image was geometrically corrected using 50 GCPs over the island and maintaining a root mean square error (RMSE) of around 3 m (approximately three quarters of a pixel). Also, the GPS was placed at the center position of each target to estimate the target position accurately so that the corresponding points can be found in IKONOS image.

Simulation of at-satellite reflectance

Because dark targets were unavailable, the at-satellite reflectance for ρ_λ=0 was modelled by an RTM with reasonable water and aerosol models. Simulation of the Satellite Signal in the Solar Spectrum (5S) model enables simulation of the signal observed by a satellite sensor for a lambertian target at sea level altitude. It took into account the effects of gaseous absorption, scattering by molecules and aerosols. Input parameters, mainly observation geometry, atmospheric conditions, ground reflectance and spectral conditions, were proposed from standard models or had to be defined by the user.

The parameters of IKONOS image were input to the model, and the at-satellite reflectance for ρ_λ=0 in each IKONOS band was simulated (Table 4).

Table 4 At-satellite reflectance for ρ_λ=0 simulated by 5S model

IKONOS spectral bands	At-satellite reflectance (%)
Blue	11.66
Green	6.81
Red	4.70
NIR	2.63

RESULTS AND DISCUSSION

The mean of surface reflectance was calculated from spectra of each target. The reflectance recorded by the sensor was extracted from the image by averaging the values of 3~4 pure pixels associated with each target. Care should be taken to avoid mixed pixels (Karpouzli and Malthus, 2003).

The REL method was employed using the IKONOS spectra reflectance and modelled reflectance for ρ_λ=0 as the independent variable and the ground measured reflectance and ρ_λ=0 as the dependent variable, and four linear regression equations for four IKONOS bands were derived (Fig.2).

The coefficients of determination for the visible bands and near-infrared band were all greater than 0.97. The slopes of the calibration lines represent the atmospheric attenuation. As can be seen atmospheric attenuation was greatest for the blue band and decreased with increasing band wavelength; the interception of the calibration lines with the *x*-axis represents the atmospheric path radiance (Smith and Milton, 1999). As can be observed the path radiance was greatest for the blue band and decreased with in-

creasing band wavelength, due to greater scattering by the atmosphere, which agree with the finding of Karpouzli and Malthus (2003).

Validation of REL method

To assess the error in the empirical relationships derived, 5 validation targets were used. The reflectance values for each target were calculated from the ground spectral measurements in the same way as that for the calibration targets; the reflectance was extracted from the image by averaging the values of 3~5 pure pixels associated with each calibration target. The predicting equations for each band were used to predict the surface reflectance. Subsequently, the predicted reflectance was compared to the actual reflectance and the difference and the relative error were calculated (Table 5).

The mean relative error between ρ_λ retrieved from IKONOS image using REL method and ground-measured ρ_λ were 10.25%, 5.94%, 4.64% and 8.03% in the IKONOS blue, green, red and near-infrared bands respectively. The relative errors were quite small for validation targets V1, V2 and V3, ranging from 1.23% to 10.45%. For the target V4, relative errors were relatively higher than those of the other targets, ranging from 6.99% to 15.91%, and were largely due to the lower reflectance of black tile on rooftop, resulting in larger relative error, even though the absolute differences between actual and predict were less than 1.52%.

CONCLUSION

The REL method yielded an empirical linear relationship between at-satellite reflectance and surface reflectance from two points: a series of bright (higher reflectance) and an estimate of at-satellite for ρ_λ through the use of an RTM with reasonable water and aerosol models. It is particularly suited for calibration of remotely sensed imagery when dark (lower reflectance) target within the image are unavailable or measurement is inconvenient.

Since the linear relationships are largely driven by the estimate of ρ_λ, care should be taken to select atmospheric, water and aerosol models as input para-

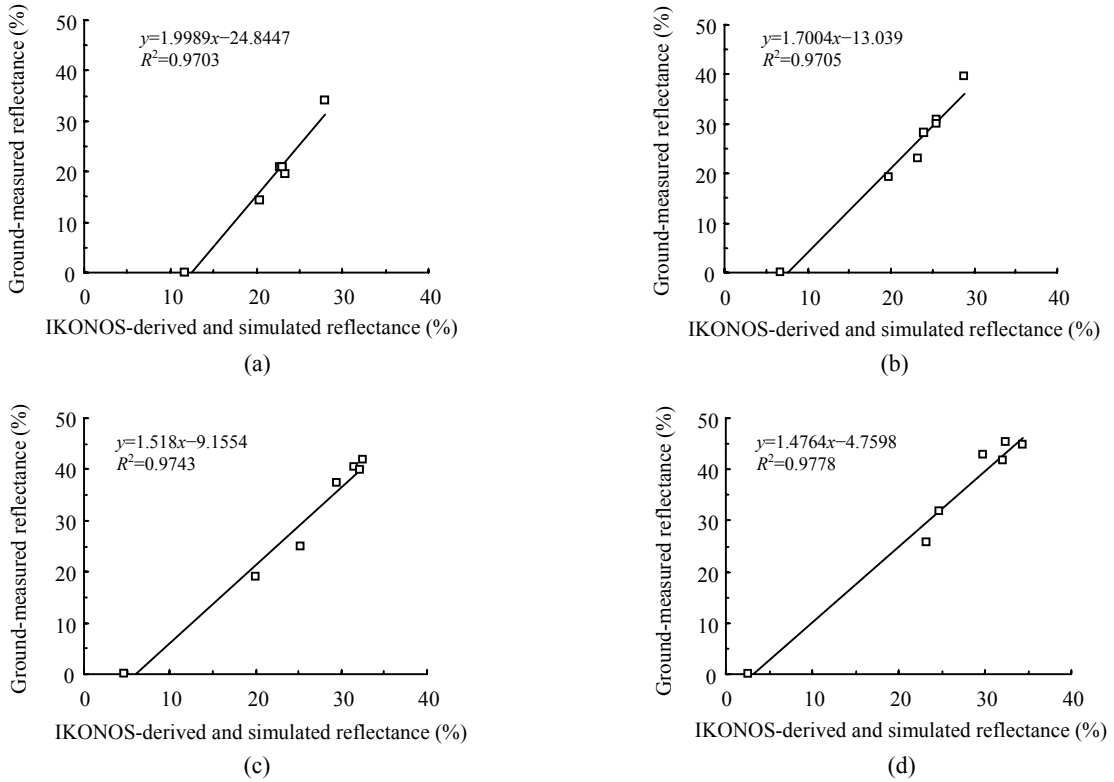

Fig.2 Linear regression equations using calibration targets and simulated data for each of the IKONOS bands. (a) IKONOS blue band; (b) IKONOS green band; (c) IKONOS red band; (d) IKONOS NIR band

Table 5 Comparison of validation targets IKONOS band reflectance (%), predicted from the refined empirical line relationships in Fig.2, and their relative error

Validation targets	IKONOS band	Actual	Predicted	Difference	Relative error (%)
V1	Blue	26.37	24.58	−1.79	6.78
V2		24.39	21.23	−3.17	12.98
V3		23.61	22.35	−1.26	5.32
V4		11.53	9.69	−1.83	15.91
V1	Green	34.84	32.94	−1.90	5.46
V2		28.49	27.25	−1.24	4.34
V3		29.52	28.93	−0.59	2.01
V4		12.69	11.18	−1.52	11.94
V1	Red	45.24	41.38	−3.86	8.53
V2		30.57	31.08	0.51	1.68
V3		33.55	33.10	−0.45	1.34
V4		13.97	12.99	−0.98	6.99
V1	NIR	52.73	47.22	−5.51	10.45
V2		33.19	33.60	0.41	1.23
V3		38.69	35.54	−3.15	8.15
V4		14.29	12.53	−1.76	12.30

meters to an RTM. Moreover, the REL targets should be stable spectrally over time when the field spectra data are not available during the satellite overpass. If the surface objects had been weathered or the physical and chemical parameters have changed, it cannot be selected as calibration and validation targets.

The large correlation coefficients observed between at-satellite reflectance and surface reflectance for the four IKONOS wavebands. Independent error assessment shown that the REL method is effective for calibrating remotely sensed data.

This study showed that the relative errors are larger than the other objects. Further works should be done to measure multiple dark targets in different region to test the accuracy of REL method and compare the results with EL methods.

ACKNOWLEDGEMENT

The author sincerely thanks Dr. Wang Fu-ming for helping with ground reflectance measurement.

References

Ben-Dor, E., Levin, N., 2000. Determination of surface reflectance from raw hyperspectral data without simultaneous ground data measurements: a case study of the GER 63-channel sensor data acquired over Naan, Israel. *International Journal of Remote Sensing*, **21**(10): 2053-2074. [doi:10.1080/01431160050021295]

Berk, A., Bernstein, L.S., Anerson, G.P., Acharya, P.K., Roberston, D.C., Chetwynd, J.H., Adler-Golden, S.M., 1998. MODTRAN cloud and multiple scattering upgrades with application to AVIRIS. *Remote Sensing of Environment*, **65**(3):367-375. [doi:10.1016/S0034-4257(98)00045-5]

Farrand, W.H., Singer, R.B., Merenyi, E., 1994. Retrieval of apparent surface reflectance from AVIRIS data: a comparison of empirical line, radiative transfer, and spectral mixture methods. *Remote Sensing of Environment*, **47**(3):311-321. [doi:10.1016/0034-4257(94)90099-X]

Ferrier, G., 1995. Evaluation of apparent surface reflectance estimation methodologies. *International Journal of Remote Sensing*, **17**(12):2291-2297.

Fleming, D., 2003. Ikonos DN Value Conversion to Planetary Reflectance. Http://www.geog.umd.edu/cress/papers/guide_dn2pr.pdf.

Karpouzli, E., Malthus, T., 2003. The empirical line method for the atmospheric correction of IKONOS imagery. *International Journal of Remote Sensing*, **24**(5):1143-1150. [doi:10.1080/0143116021000026779]

Kneizys, F.X., Shettle, E.P., Abreu, L.W., Chettwynd, J.H., Anderson, G.P., Gallery, W.O., Selby, J.E.A., Clough, S.A., 1989. User Guide to Lowtran 7. Hanscom AFB, Massachusetts, p.146.

Kruse, F.A., 1988. Use of airborne imaging spectrometer data to map minerals associated with hydrothermally altered rocks in the northern Grapenvine Mountains, Nevada and

California. *Remote Sensing of Environment*, **24**(1):31-51. [doi:10.1016/0034-4257(88)90004-1]

Matthew, M.W., Adler-Golden, S.M., Berk, A., Felde, G., Anderson, G.P., Gorodetzky, D., Paswaters, S., Shippert, M., 2002. Atmospheric Correction of Spectral Imagery: Evaluation of the FLAASH Algorithm with AVIRIS Data. Proceedings of 31st Applied Imagery Pattern Recognition Workshop. Bellingham, WA, p.157-163.

Moran, M.S., Bryanta, R., Thomeb, K., Nia, W., Nouvellona, Y., 2001. A refined empirical line approach for reflectance factor retrieval from Landsat-5 TM and Landsat-7 ETM+. *Remote Sensing of Environment*, **78**(1-2):71-82. [doi:10.1016/S0034-4257(01)00250-4]

Perry, E.M., Warner, T., Foote, P., 2000. Comparison of atmospheric modelling versus empirical line fitting for mosaicking HYDICE imagery. *International Journal of Remote Sensing*, **21**(4):799-803. [doi:10.1080/014311600210588]

Richter, R., Schläpfer, D., 2002. Geo-atmospheric processing of airborne imaging spectrometry data: Part 2. Atmospheric/topographic correction. *International Journal of Remote Sensing*, **23**(13):2631-2649. [doi:10.1080/01431160110115834]

Roger, N., Gregg, A., 2002. Surface Reflectance Calibration of Terrestrial Imaging Spectroscopy Data: a Tutorial Using AVIRIS. Http://popo.jpl.nasa.gov/docs/workshops/02_docs/ 2002_Clark_web.pdf.

Smith, G.M., Milton, E.J., 1999. The use of the empirical line method to calibrate remotely sensed data to reflectance. *International Journal of Remote Sensing*, **20**(13):2653-2662. [doi:10.1080/014311699211994]

Tanre, D., 1990. Description of a computer code to simulate the satellite signal in the solar spectrum: 5S code. *International Journal of Remote Sensing*, **11**(4):659-668.